Journal of Fluids and Structures (1998) **12,** 171–181

PRESSURE MEASUREMENTS AROUND A TWO-DIMENSIONAL GAUZE AT INCIDENCE

A. Ito

Department of Mechanical Engineering, School of Science and Technology, Meiji University 1-1-1 Higashi-Mita, Tama-ku, Kawasaki 214, Japan

AND

K.P. Garry

College of Aeronautics, Cranfield University, Bedford MK43 OAL, U.K.

(Received 6 May 1997 and in revised form 3 November 1997)

Measurements of the static pressure near a 2-D plane gauze, of aspect ratio 2, are presented for a series of open-jet wind-tunnel tests at chord Reynolds numbers in the range $1{\cdot}12 \times 10^5$ to $2{\cdot}69 \times 10^5$. The gauze was woven from nylon monofilament, in a square mesh, resulting in a porosity of 37% and a resistance coefficient of 3·8. Measurements were taken from static pressure tappings in an end-plate, close to the gauze, for angles of incidence in the range 15°–90°. The flow pattern through the gauze is also investigated, using a 2-D smoke flow-visualization wind tunnel. Lift and drag on the gauze section are measured using a force balance and seen to be in good agreement with loads derived from integrating the static pressure signature. The chordwise variation of static pressure around the gauze section is seen to be of a similar form to that for a flat plate. Mean values of the pressure-coefficient distribution for the gauze are displaced from those for the flat plate by amounts that are dependent on incidence.

1. INTRODUCTION

It is known that two-dimensional expansion of a free-stream flow occurs due to the resistance of a gauze. The relationship between gauze porosity and drag was first studied theoretically by Taylor (1944) using a simple source flow model to replace the gauze. This technique showed good agreement with experimental results at low resistance coefficients, see Taylor & Davies (1944). More recent work by Koo & James (1973) has improved Taylor's source model, extending its application to gauze resistance coefficients of up to 10; experimental and numerical data agree well for the velocity profile downstream of the gauze. Work by the co-author, Ito (1974, 1981, 1986), using a revised Taylor source model, has shown good agreement between the predicted expansion profile and that visualized in the Meiji University low-speed smoke flow-visualization wind tunnel. This revised model was also used to demonstrate the design of two-dimensional diffusers using gauzes. In order to analyse the validity of the various source models, it becomes important to understand the detailed pressure distribution around a gauze. Consequently, results from a series of wind-tunnel tests are presented relating to pressure measurements around a nylon-filament gauze with a resistance coefficient, k_n, of 3·8.

0889-9746/98/020171 + 11 $25.00/fl970134

2. RESISTANCE COEFFICIENT OF THE GAUZE

The gauze chosen for the tests was a 30 strands-per-inch, square-mesh, woven nylon monofilament with a mean diameter of 0·354 mm and porosity (open area ratio), β, of 37%; see Figure 1. An initial series of measurements were carried out in the closed working section of a simple blower tunnel, with a cross-sectional area of 0.01 m^2, to establish the resistance coefficient k_n of the gauze, defined by

$$k_n = \frac{\Delta P}{\frac{1}{2}\rho U_n^2},$$

where U_n is the uniform air velocity in the blower tunnel, ρ the air density and Δp the static pressure drop across the gauze.

Values of resistance coefficient k_n for free-stream speeds ranging from 1·5 to 17 m/s are given in Figure 2. The corresponding test Reynolds numbers, (Re), based on the monofilament diameter, d_m, are in the range 36–409.

The variation of test-section wall-centreline static pressure coefficient, C_p, upstream and downstream of the gauze, given in Figure 3, shows only a small dependence on Reynolds number. The region within which the change in static pressure occurs across the gauze Δp is clearly evident from Figure 3. This variation should be considered when analysing the chordwise static pressure distribution around the gauze in the following section.

3. PRESSURE DISTRIBUTION AROUND THE GAUZE

3.1. Experimental Arrangement

Measurements of the static pressure variation around the gauze were carried out in the College of Aeronautics "Weybridge" wind tunnel. This facility has a closed return circuit

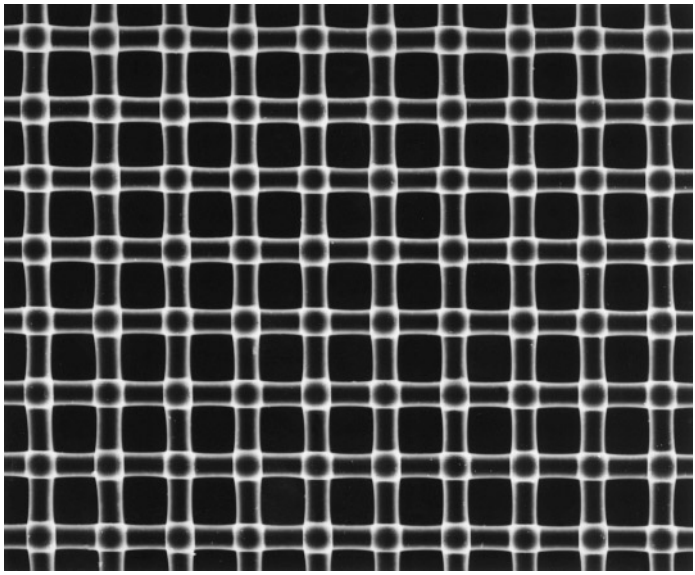

Figure 1. The 30 strands-per-inch nylon monofilament square mesh gauze.

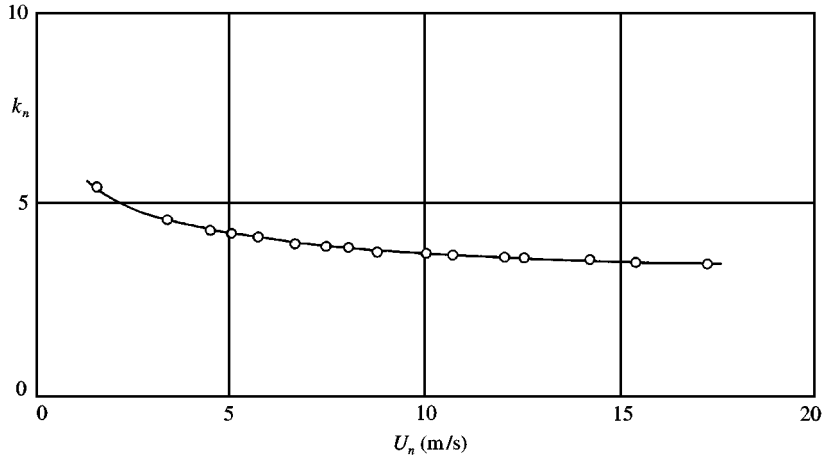

Figure 2. Resistance coefficient, k_n, curve for the gauze tested.

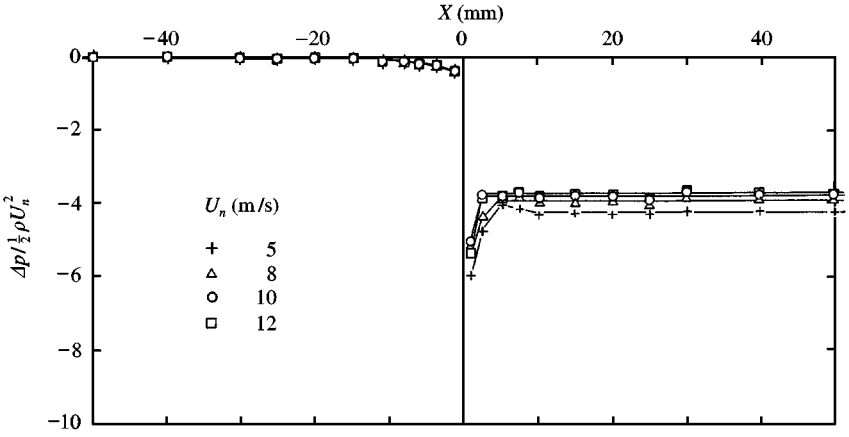

Figure 3. Variation of pressure distribution across the gauze, at $\alpha = 90^\circ$, with U_n and hence Reynolds number.

and an open working section with an exit nozzle diameter of 1·06 m. A detailed arrangement of the test apparatus is given in Figure 4. The section of gauze under test has a chord, b, of 200 mm and a span, h, of 400 mm and is mounted, spanwise vertically, in the working section at incidence angles in the range of 15°–90° in steps of 15°. In order to ensure essentially two-dimensional flow, a circular end-plate, with a diameter of 1000 mm is mounted at each end of the gauze. Each end-plate has a central slot, 1 mm wide and 200 mm long, through which the gauze is passed, and clamped to both top and bottom end-plates by angle brackets; see Figure 4(c). The lower clamp is designed to allow the gauze to be held in tension during each test simply by hanging a distributed 18 kg load from the end. Any gaps between the gauze and the upper end-plate are filled with silicone sealant. Along both sides of the slot on the upper end-plate, a total of 42 static pressure tappings of 0.5 mm internal diameter are arranged at 10 mm intervals. Each row of pressure tappings is displaced by

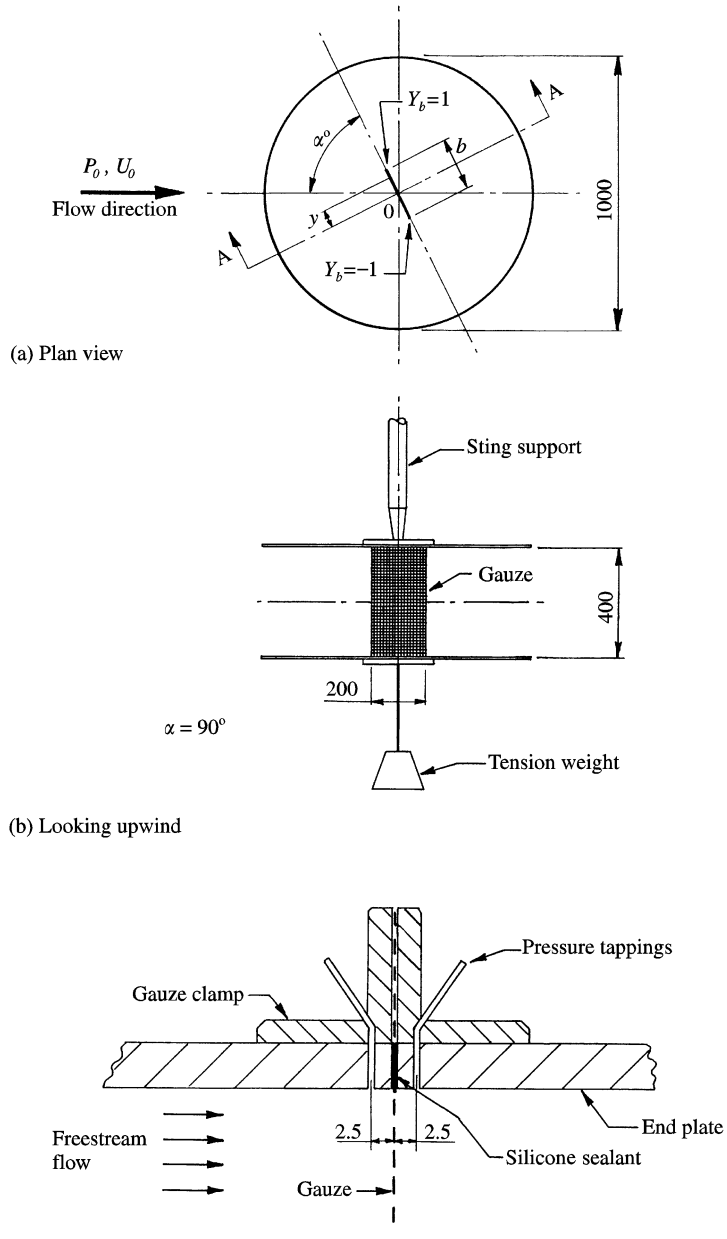

Figure 4. Mounting arrangement for the 2-D gauze section in the open jet wind tunnel: (a) plan view; (b) rear view, $\alpha = 90°$; (c) magnified cross-section of the pressure tapping installation. All dimensions in mm, $Y_b = y/(b/2)$.

2·5 mm from the centre plane of the gauze, which corresponds to a distance of 7·06 d_m, where d_m is the diameter of the monofilament of the gauze tested.

The wind-tunnel dynamic pressure is measured by a Pitot-static tube located on the axial centerline of the nozzle at the entrance to the working section. Differences between local

static pressure, p, at each of the 42 tappings and reference static pressure, p_0, were measured by a differential pressure transducer coupled to a 48-port D-type Scanivalve, controlled, together with the data collection, by a microcomputer.

3.2. Gauze Pressure Distribution

Initial tests were concerned with the effects of a variation in Reynolds number Re for the gauze mounted at $\alpha = 90^\circ$. Reynolds numbers of $1{\cdot}12 \times 10^5$, $1{\cdot}63 \times 10^5$, $2{\cdot}18 \times 10^5$ and $2{\cdot}68 \times 10^5$, based on gauze chord b, were considered, which correspond to free-stream velocities, U_0, in the range of 8·2–19·8 m/s.

The variation of pressure coefficient, $C_p = (p - p_0)/q$, where $q = \frac{1}{2}\rho U_0^2$, with a nondimensional chordwise position, $y/(b/2)$, for each Reynolds number tested at $\alpha = 90^\circ$, is shown in Figure 5. It can be seen that the influence of Reynolds number is small, with the exception of the lowest value tested. The chordwise variation in C_p upstream of the gauze is continuous as expected, while that downstream is seen to be discontinuous. This may be due to flow instability through the gauze since its porosity, β, is below the critical value of 0.57, for which a chordwise periodical flow instability has been shown to occur (Bradshaw 1965). Integration of the chordwise pressure distribution makes it possible to evaluate the

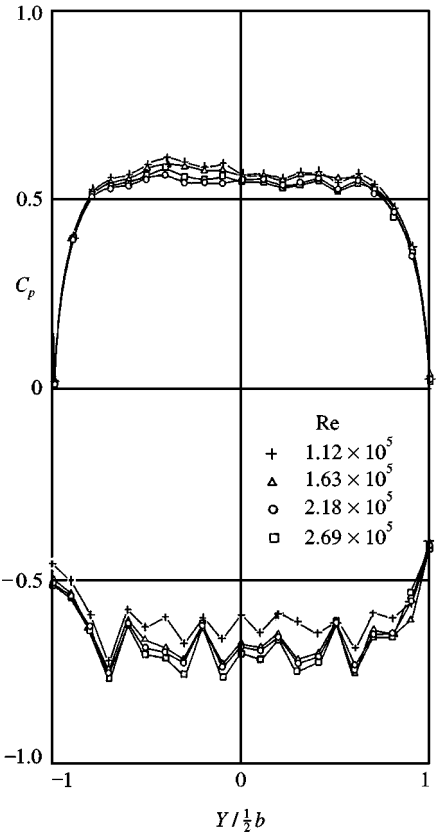

Figure 5. Variation of the chordwise pressure distribution at $\alpha = 90^\circ$ with Reynolds number.

aerodynamic force on the gauze. Values of drag coefficient ($C_D = D/qS$, where $S = bh$) versus k_n for each Reynolds number tested are given in Table 1.

Values of C_p versus $y/(b/2)$ for the gauze at incidence angles, α, in the range 15°–90° and at a Re $= 2{\cdot}17 \times 10^5$ ($U_0 = 16$ m/s) are given in Figure 6. As in the $\alpha = 90°$ case shown in Figure 5, the C_p variation upstream of the gauze shows both a movement and change in magnitude of the C_p distribution consistent with the change in incidence.

TABLE 1
Resistance and drag coefficients for the $\alpha = 90°$ gauze

Re	k_n	C_D
$1{\cdot}12 \times 10^5$	4·1	1·12
$1{\cdot}63 \times 10^5$	3·8	1·16
$2{\cdot}18 \times 10^5$	3·5	1·14
$2{\cdot}69 \times 10^5$	3·5	1·16

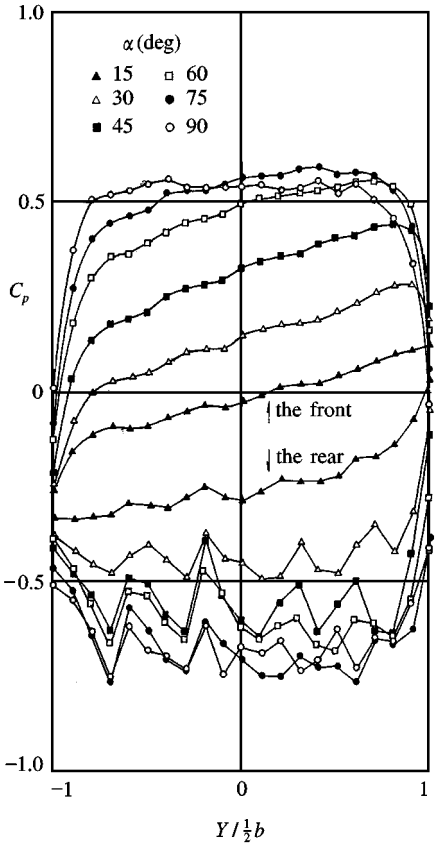

Figure 6. Variation of the gauze chordwise pressure distribution with incidence; $U_0 = 16$ m/s, Re $= 2{\cdot}18 \times 10^5$.

3.3. Estimation of Oblique Gauze Resistance Coefficient

Values of gauze resistance coefficient, k_n, at each Reynolds number and incidence angle α are evaluated as follows:

(i) a local flow velocity immediately upstream of the gauze, w, is calculated using the relation

$$\frac{w}{U_0} = (1 - C_p)^{0.5},$$

from the application of the incompressible form of Bernoulli's theorem to the streamline passing through the centre of the gauze, where $y = 0$;

(ii) taking the velocity component normal to the gauze U_n where $y = 0$, to be given by $U_n = w \sin \alpha$, corresponding values of k_n can be taken from Figure 2.

The variation of the resistance coefficient k_n with incidence is given in Table 2; k_n is seen to increase as incidence is reduced.

Values of drag coefficient, $C_D = D/qs$, and lift coefficient, $C_L = L/qs$, derived from the pressure distribution, for each angle α at a $\mathrm{Re} = 2{\cdot}17 \times 10^5$ ($U_0 = 16$ m/s), are given in Table 2.

3.4. Comparison with Flat-Plate Pressure Distribution

A comparison of the C_p distribution between the gauze at $\mathrm{Re} = 2{\cdot}17 \times 10^5$ and that of a flat plate at $\mathrm{Re} = 1{\cdot}57 \times 10^5$, taken from Fage & Johansen (1927), is shown in Figure 7. The gauze pressure distribution is seen to approach that of the flat plate as the resistance coefficient increases.

In addition, the average pressure coefficient on the front of the gauze, C_{pf}, and the average pressure coefficient on the rear of the gauze, C_{pr}, are evaluated, and these values are compared in Figure 8 with the average front and rear pressure coefficients for the flat plate. Values of C_{pf} for the gauze are seen to be displaced from that of the flat plate by a virtually constant value across the incidence range tested. The average pressure coefficient downstream of the gauze is greater than that for the plate and the difference between plate and gauze is seen to increase as incidence is increased. This is assumed to be due to both the flow through the gauze and the difference in shear layer curvature increasing the near-wake pressure of the gauze.

TABLE 2
Resistance, lift and drag coefficients for the oblique gauze at $\mathrm{Re} = 2{\cdot}18 \times 10^5$

α (deg)	k_n	C_L	C_D
15	4·4	0·22	0·06
30	3·9	0·48	0·27
45	3·8	0·59	0·59
60	3·7	0·51	0·88
75	3·7	0·30	1·12
90	3·6	0	1·14

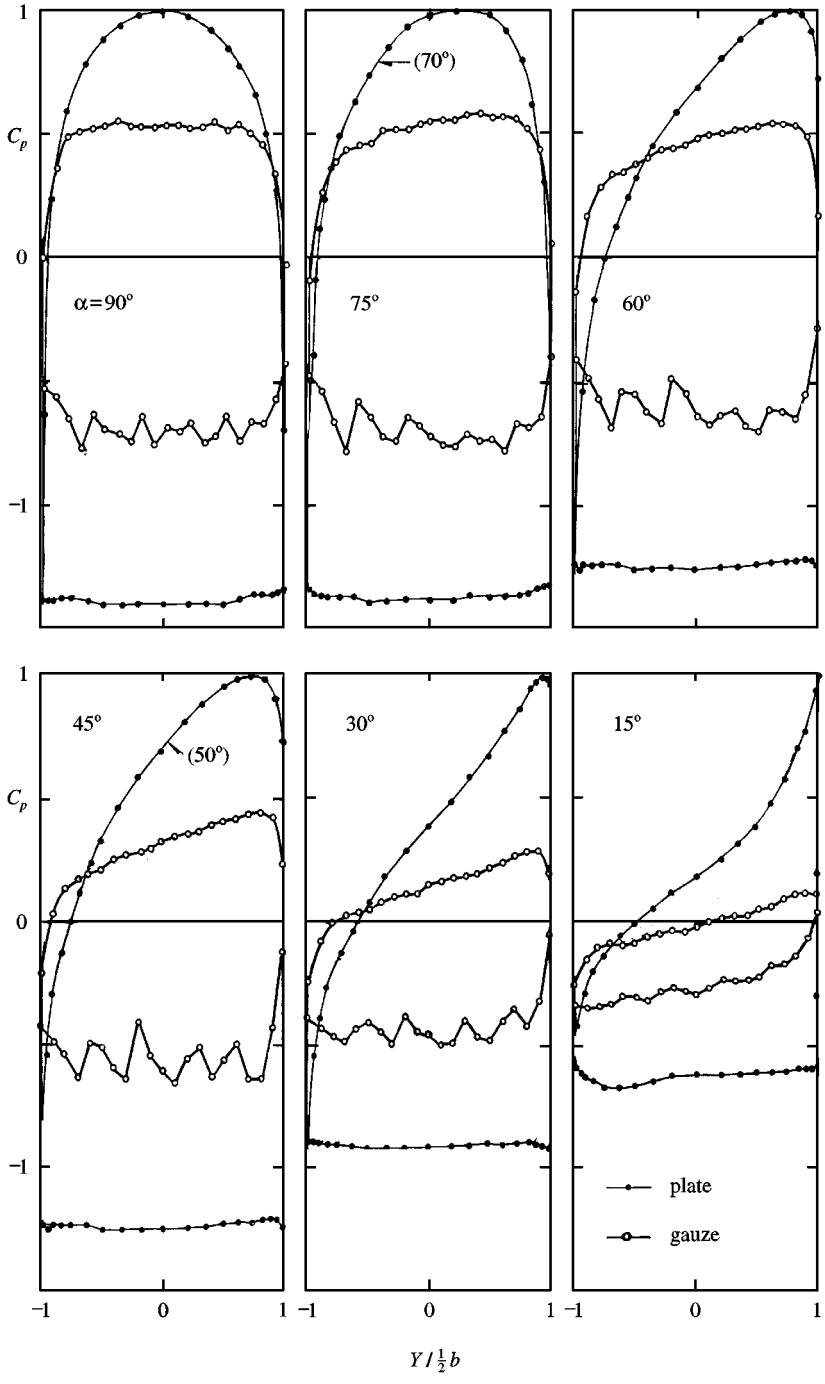

Figure 7. Comparison of the variation of chordwise pressure distribution for the gauze ($Re = 2{\cdot}17 \times 10^5$) and a flat plate ($Re = 1{\cdot}57 \times 10^5$).

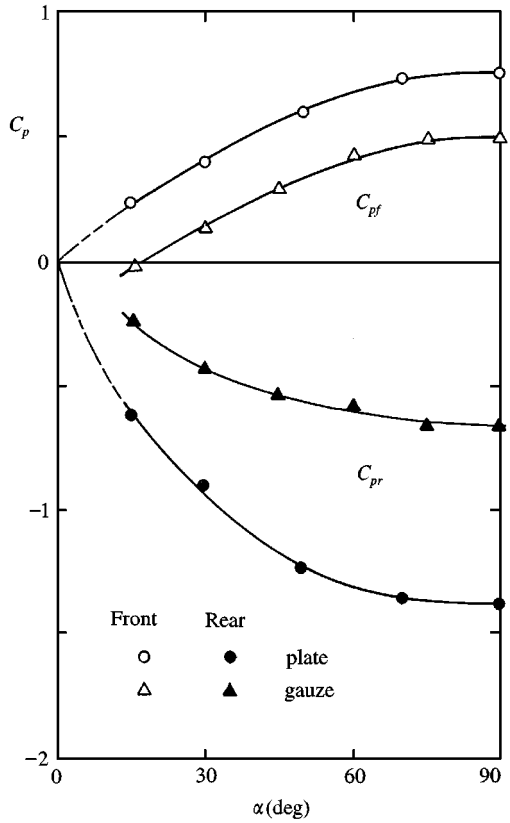

Figure 8. Variation of the average upstream pressure coefficient, C_{pf}, and downstream pressure coefficient, C_{pr}, for the gauze and flat plate.

4. SMOKE WIND TUNNEL TESTS

4.1. Flow Visualization

Photographs of the flow pattern through the gauze, using the Meiji University smoke flow-visualization wind tunnel Yamana & Akuzawa (1971), are shown in Figure 9. The wind-tunnel test-section is 1500 mm high and 200 mm wide. The gauze has a chord of 300 mm and spans the test-section centreline at a free-stream velocity U_0 of 8·4 m/s, $\mathrm{Re} = 1{\cdot}71 \times 10^5$. It can be seen that a 2-D expansion of the flow occurs uniformly around the gauze, as anticipated.

By assuming a 2-D expansion of the streamtube which contains the gauze, mean values of the velocity component normal to the gauze U_n can be evaluated from each photograph, using continuity theory. The corresponding values of resistance coefficient k_n can be taken from Figure 2 and are given in Table 3. This approach ensures that the large changes in Reynolds number that occur at lower incidence are allowed for in the final k_n values. The variation of resistance coefficient k_n evaluated in this way is consistent with that derived from the open-jet wind-tunnel tests.

TABLE 3
C_L and C_D coefficients of the oblique gauze by the balance of the Meiji smoke wind tunnel at $\mathrm{Re} = 1{\cdot}71 \times 10^5$

α (deg)	k_n	C_L	C_D
15	5·3	0·22	0·16
30	4·8	0·41	0·33
45	4·5	0·55	0·67
60	4·4	0·48	0·96
75	4·3	0·30	1·12
90	4·2	0	1·22

4.2. FORCE MEASUREMENTS

In order to verify the gauze lift and drag coefficients derived from the pressure distribution measurements, tests were made using a force balance in the smoke flow-visualization wind tunnel at $\mathrm{Re} = 1{\cdot}71 \times 10^5$ ($U_0 = 8{\cdot}4$ m/s). A section of gauze with a chord of 300 mm was held between thin, circular end-plates, of diameter 350 mm. The end-plates were held 194 mm apart by four cylindrical rods and the assembly mounted centrally in the smoke wind-tunnel working section on an external force balance. This arrangement minimizes the influence of the wind-tunnel-wall boundary layer. In order to establish the gauze lift and drag coefficient, measurements of axial load on the assembly were made, both with and without the gauze, to establish the aerodynamic force of the gauze section alone at each incidence.

Data for gauze lift, C_L, and drag, C_D, coefficients versus k_n are given in Table 3 and presented graphically in Figure 10. These data are in agreement with that derived from the pressure distribution, and some similarity with the C_L and C_D variation with incidence, α, for the flat plate is apparent; see Figure 10.

5. CONCLUSIONS

Pressure measurements around a nylon-mesh gauze with a porosity of 37% and resistance coefficient of 3·8 for incidence angles in the range 15°–90° in 2-D flow, are presented for Reynolds numbers, based on gauze chord, in the range $1{\cdot}12 \times 10^5$ to $2{\cdot}69 \times 10^5$.

The expansion profile of the flow around gauze was visualized using a 2-D smoke wind-tunnel, and values of lift and drag coefficients for each oblique gauze were also measured using a force balance. It is shown that values of C_L and C_D, derived from the pressure distribution around the gauze, are in good agreement with that obtained from force balance measurements. In addition, the variation of both C_L and C_D with incidence α is shown to be similar to that for a 2-D flat plate.

Further work is needed to establish both the influence of the displacement of the static pressure tappings from the gauze surface and the applicability of these results for one mesh type to other mesh configurations.

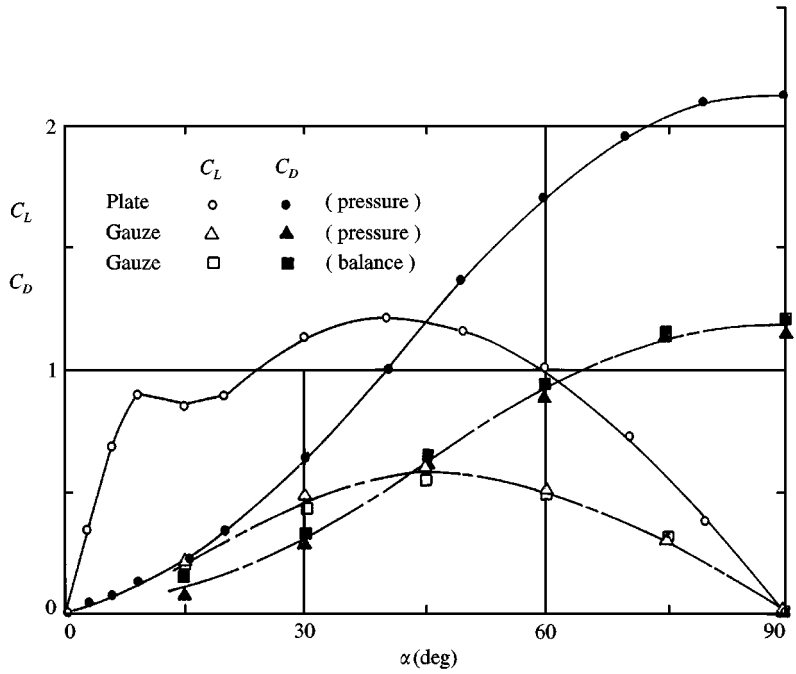

Figure 10. Comparison of the variation of lift and drag coefficients C_L and C_D respectively, with incidence α, for both the gauze and flat plate.

REFERENCES

Bradshaw, P. 1965. The effect of wind-tunnel screens on nominally two-dimensional boundary layers. *Journal of Fluid Mechanics*, **22**, 679–687.

Fage, A & Johansen, F. C. 1927. On the flow of air behind an inclined flat plate of infinite span. *Proceedings of the Royal Society of London* A **116**, 170–197.

Ito, A. 1974. The expansion of flow due to the resistance of a wire gauze, *Transactions of Japan Society of Aeronautics and Space Science* **22**, 373–377.

Ito, A. 1981. Expansion of flow due to the resistance of an oblique wire gauze, *Transactions of Japan Society of Aeronautics and Space Science* **29**, 248–253.

Ito, A. 1986. Expansion of flow due to resistance of a wire gauze placed in a parallel sided channel. *Transactions of Japan Society of Aeronautics and Space Science* **34**, 308–315.

Koo, J. K. & James, D. F. 1973. Fluid flow around and through a screen. *Journal of Fluid Mechanics* **60**, 513–538.

Taylor, G. I. 1944. Air resistance of a flat plate of very porous material. ARC R&M 2236.

Taylor, G. I. & Davies, R. M. 1944. The aerodynamics of porous sheets. ARC R&M 2237.

Yamana, M. & Akuzawa, S. 1971. Blow-down type smoke wind tunnel, *Transactions of Japan Society of Aeronautics and Space Science* **19**, 331–335.

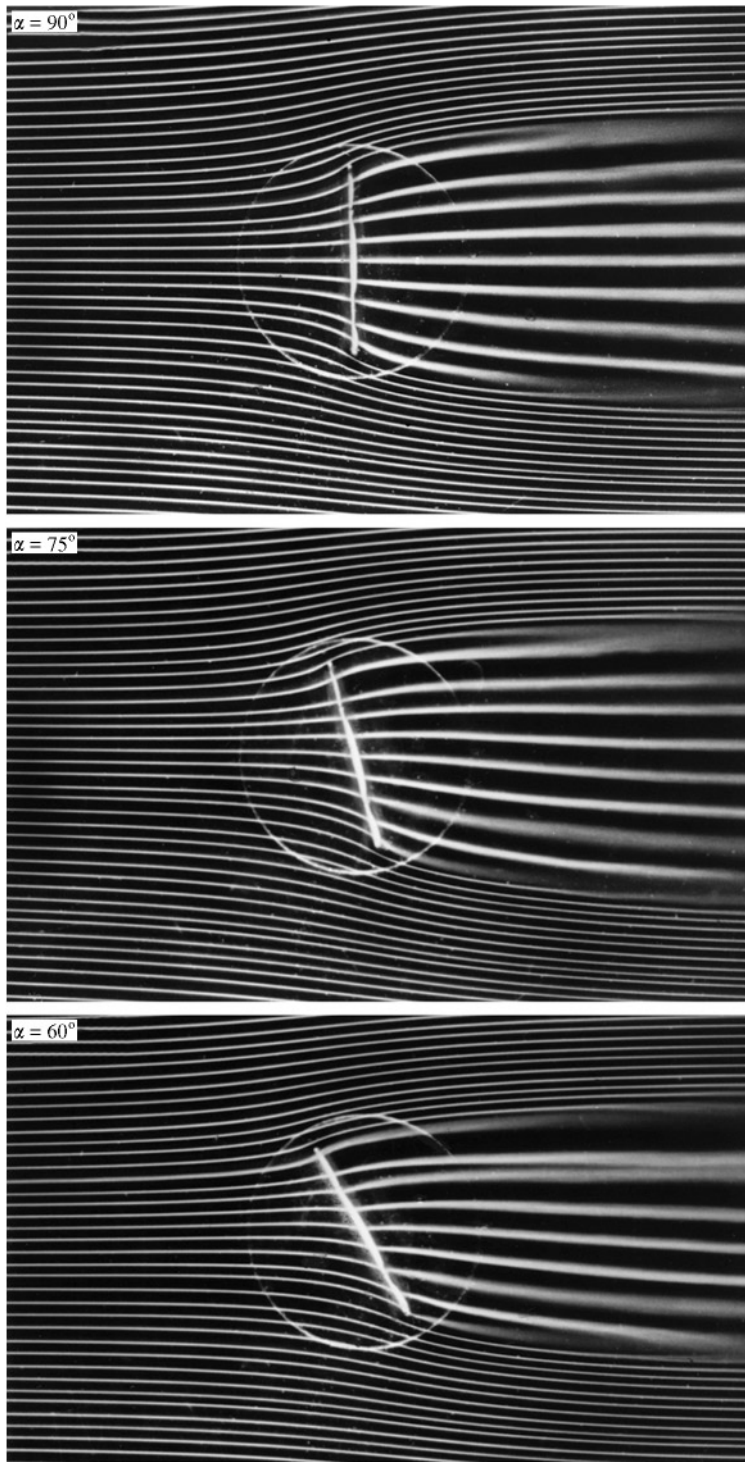

(a)

Figure 9. (a) Flow pattern around the gauze at $Re = 1{\cdot}17 \times 10^5$ using the 2-D Meiji University smoke flow visualization wind tunnel for $\alpha = 90^\circ$, 75° and 60° (b). $\alpha = 45^\circ$, 30° and 15°.

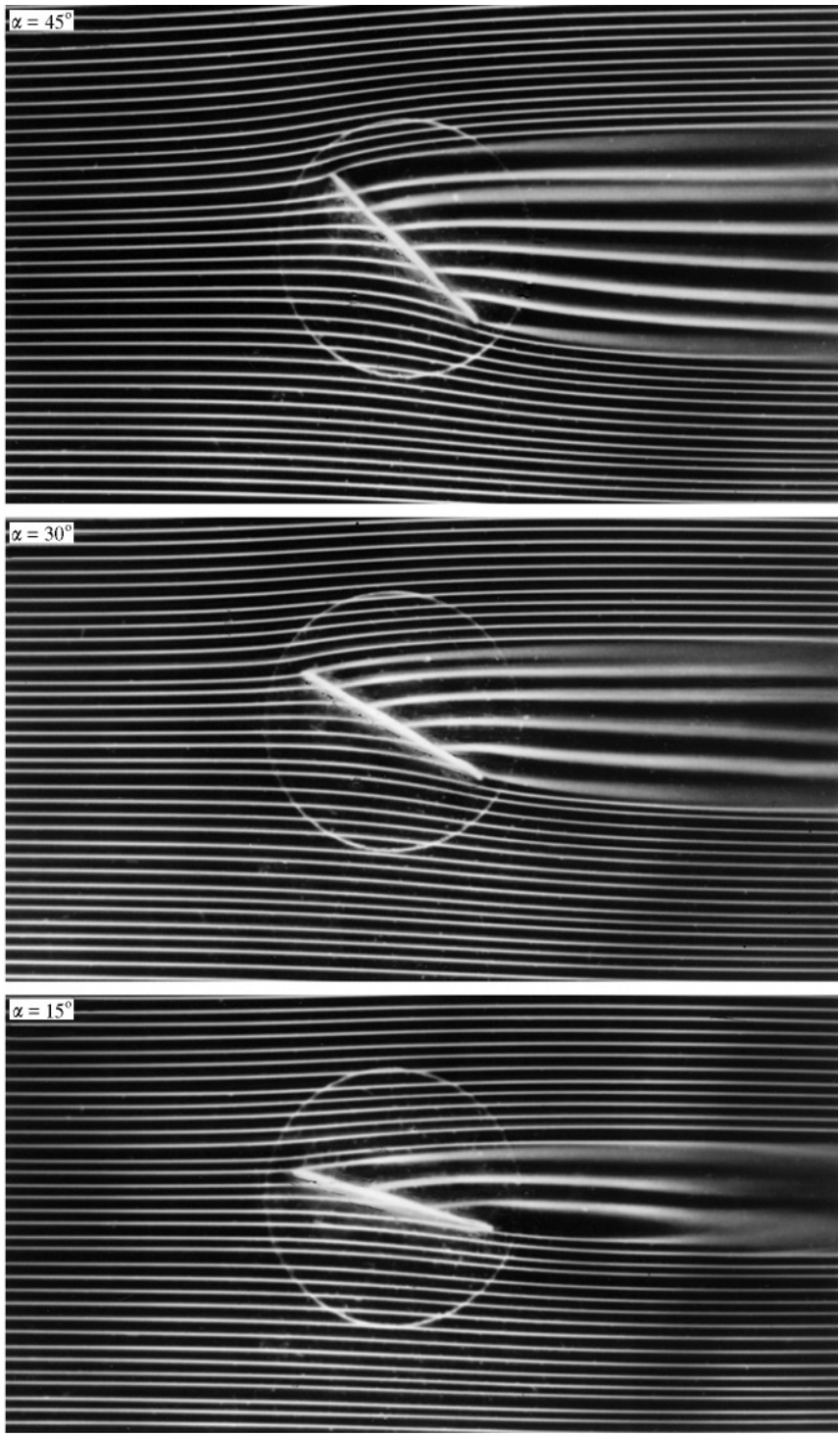

(b)

Figure 9. (*Continued*).